J. Fluid Mech. (2023), *vol*. 954, A50, doi:10.1017/jfm.2022.1022

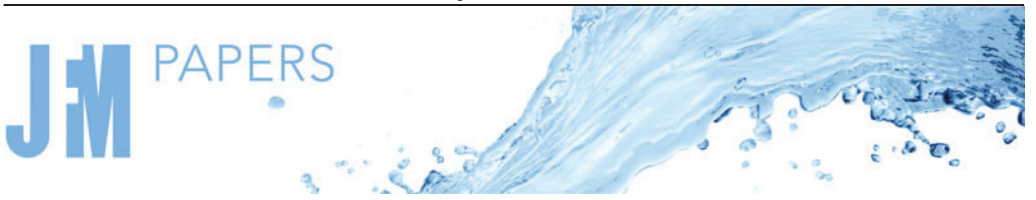

Enhanced extreme wave statistics of irregular waves due to accelerating following current over a submerged bar

Jie Zhang[1], **Yuxiang Ma**[1,†], **Ting Tan**[1], **Guohai Dong**[1] **and Michel Benoit**[2,3]

[1]State Key Laboratory of Coastal and Offshore Engineering, Dalian University of Technology, Dalian 116023, PR China

[2]EDF R&D, Laboratoire National d'Hydraulique et Environnement (LNHE), Chatou 78400, France

[3]LHSV, Ecole des Ponts, EDF R&D, Chatou 78400, France

(Received 1 July 2022; revised 1 December 2022; accepted 1 December 2022)

We present experimental results of irregular long-crested waves propagating over a submerged trapezoidal bar with the presence of a background current in a wave flume. We investigate the non-equilibrium phenomenon (NEP) induced by significant changes of water depth and mean horizontal flow velocity as wave trains pass over the bar. Using skewness and kurtosis as proxies, we show evidence that an accelerating following current could increase the sea-state non-Gaussianity and enhance both the magnitude and spatial extent of the NEP. We also find that below a 'saturation relative water depth' $k_p h_2 \approx 0.5$ (k_p being the peak wavenumber in the shallow area of depth h_2), although the NEP manifests, the decrease of the relative water depth does not further enhance the maximum skewness and kurtosis over the bar crest. This work highlights the nonlinear physics according to which a following current could provoke higher freak wave risk in coastal areas where modulation instability plays an insignificant role.

Key words: topographic effects, surface gravity waves

1. Introduction

Extreme waves with crest-to-trough excursions higher than twice the significant wave height are referred to as 'freak waves' or 'rogue waves' (e.g. Dysthe, Krogstad & Müller 2008). Although different mechanisms have been put forward (Kharif & Pelinovsky 2003; Onorato *et al.* 2013; Adcock & Taylor 2014), a universal explanation of freak wave formation in the context of ocean waves is still under debate (Akhmediev & Pelinovsky 2010; Fedele *et al.* 2016; Dematteis *et al.* 2019).

† Email address for correspondence: yuxma@dlut.edu.cn

As a new perspective of nonlinear focusing, the non-equilibrium dynamics (NED) provoked by an abrupt change of environmental conditions has received considerable attention in the last few years (e.g. Onorato & Suret 2016; Trulsen 2018). It provides some generality in explaining freak wave formation in coastal areas, where the well-known modulation instability (MI) introduced by Benjamin (1967) may be restrained (Voronovich, Shrira & Thomas 2008; Kharif *et al.* 2010). The pioneering investigation of NED effects induced by significant depth change was conducted by Trulsen, Zeng & Gramstad (2012). Using skewness and kurtosis as proxies, they showed that non-Gaussian behaviour and freak wave occurrence probability are locally enhanced shortly after a submerged slope. Recent studies have investigated various factors affecting the sea-state non-equilibrium responses. The relative water depth in the shallower area plays the dominant role (Zeng & Trulsen 2012; Trulsen *et al.* 2020): it should be lower than a threshold for the NED to manifest. Other factors, including the incident significant wave height (Zheng *et al.* 2020; Zhang, Benoit & Ma 2022), the spectral width (Ma, Ma & Dong 2015), the wave direction (Ducrozet & Gouin 2017; Ma *et al.* 2017) and the shape of the bathymetry (Gramstad *et al.* 2013; Kashima & Mori 2019; Zheng *et al.* 2020; Lawrence, Trulsen & Gramstad 2022) also influence the sea-state dynamical responses. For out-of-equilibrium sea states, the wave kinematics (Lawrence, Trulsen & Gramstad 2021; Zhang & Benoit 2021) as well as the sea-state equilibration process on a long spatial scale (Zhang *et al.* 2019, 2022) have been studied. From a theoretical perspective, the intensified freak wave probability provoked by significant depth variations could be described by the stochastic model of Li *et al.* (2021*b*) which is built based on the second-order deterministic model (Li *et al.* 2021*a*,*c*), or by the stochastic model for non-homogeneous processes introduced in Mendes *et al.* (2022).

In addition to bathymetry variations, currents and tides play significant roles in wave evolution in coastal areas (Longuet-Higgins & Stewart 1961; Peregrine 1976), and could lead to freak wave formation (Lavrenov & Porubov 2006). Here, we limit ourselves to discuss the case of horizontally non-homogeneous currents without evident vertical shear effect (i.e. the mean horizontal flow velocity varies in the horizontal direction x, yet the profile of the horizontal velocity remains more or less uniform in the vertical direction). The sheared currents as well as the current-induced vorticity are important for freak wave formation (e.g. Hjelmervik & Trulsen 2009; Curtis & Murphy 2020), and are left for future investigation.

In the linear regime, an adverse current could refract waves and form spatial wave-focusing locations (caustics); such freak waves can be well predicted by the ray theory (White & Fornberg 1998). In the nonlinear regime, ambient currents could change the freak wave probability via affecting the wave steepness. When propagating over a current with adverse gradient in horizontal velocity (i.e. accelerating opposing current or decelerating following current), wave steepness is enhanced. The wave nonlinearity is therefore increased, promoting the destabilization of the wave train (Gerber 1987; Stocker & Peregrine 1999) and the occurrence of a frequency downshift (Chawla & Kirby 2002; Ma *et al.* 2010). Furthermore, the criterion for the manifestation of MI is altered due to the current (Liao *et al.* 2017), so that MI may occur in wave trains that are considered stable in quiescent water. The role of an opposing current in triggering freak waves as a result of MI has been confirmed for long-crested deep-water waves (Onorato, Proment & Toffoli 2011; Toffoli *et al.* 2013; Ducrozet *et al.* 2021), and for short-crested waves over opposing currents that are either normal or oblique to the mean wave propagation direction (Toffoli *et al.* 2011, 2015). However, MI ceases to manifest anyway below a threshold depth that is corrected by considering the current effects, so that the wave–current interaction as

a nonlinear mechanism of freak wave formation becomes ineffective for coastal waves and currents in sufficiently shallow water.

Most studies attribute the enhanced freak wave probability to the MI reinforced by opposing currents, and consider that following currents would reduce the freak wave probability as they weaken the MI. But this conclusion deserves to be investigated in the circumstances where the MI does not dominate the wave evolution. In analogy to the depth variation, the inhomogeneity of the current field may also result in NED (Trulsen 2018) and increase the freak wave probability, but there is no experimental evidence of this mechanism yet. In this study, we show experimental results of unidirectional irregular waves propagating over horizontally non-homogeneous media, where the water depth and the following current velocity change in the direction of wave propagation. Our main goal is to provide experimental evidence that an accelerating following current can lead to NED and, counter-intuitively, increase the freak wave occurrence without the effects of MI. In addition, we further discuss the saturation relative water depth for enhancing the magnitude of NED.

The remainder of this article is organized as follows. The experimental set-up and test conditions are described in § 2. The experimental results are analysed in § 3, discussing the effects induced by an accelerating following current, and the evolution of the maximum values of the statistical wave parameters achieved over a bar crest as functions of relative water depth. Conclusions are summarized in § 4.

2. Experimental set-up

The experiments were conducted in the wave–current flume of the National Marine Environmental Monitoring Center in Dalian, China. The flume, with total length $l = 80\,\mathrm{m}$ and width $b = 1.5\,\mathrm{m}$, is equipped with a piston-type wave maker on one side and a passive dissipation zone on the other. The current is generated with a pump, and the flow inlet is placed 2 m after the wave maker and the outlet 1 m before the damping zone.

Four experimental configurations are considered. The two main ones involved a submerged trapezoidal bar and irregular waves, without any current (denoted UWO for ‘uneven bottom with waves only’) or with a following current (denoted UWC for ‘uneven bottom with waves and current’). Additional tests were conducted with the bar and only the following current (denoted UCO for ‘uneven bottom with current only’) for validation. Finally, wave tests with the bar removed and no current (denoted FWO for ‘flat bottom with waves only’) were performed for comparative purposes.

The water depth close to the wave maker is fixed at $h_1 = 1\,\mathrm{m}$ throughout the campaign. The submerged bar starts 17.3 m away from the wave maker, and consists of an 18 m long upslope (1/30), a 10 m long bar crest and a 12 m long downslope (−1/20). The origin of the x abscissa is defined at the toe of the upslope. Over the bar crest, the water depth is decreased to $h_2 = 0.4\,\mathrm{m}$. The relatively mild upslope is chosen to diminish the vorticity of the flow that could be generated by the depth variation. The waves were measured by capacitance-type probes with a sampling frequency of 50 Hz. In the UWO and UWC tests, 33 wave probes were set with 2 m spacing before and over the upslope, 1 m spacing close to the bar crest and 4 m spacing after the bar. In the FWO tests, 16 probes were arranged with 2 m spacing in the area where the bar was installed. The layout of the two seabed configurations and the corresponding arrangements of the probes are shown in figure 1.

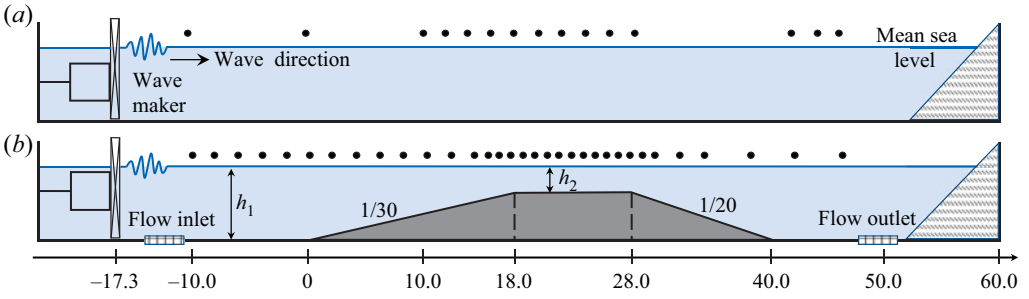

Figure 1. Sketch of the experimental set-ups and the locations of wave probes (filled black circles) for (*a*) the FWO tests and (*b*) the UCO, UWO and UWC tests.

The incident wave trains are generated considering a JONSWAP-type spectrum $S(f)$:

$$S(f) = \frac{\alpha g^2}{(2\pi)^4 f^5} \exp\left[-\frac{5}{4}\left(\frac{f_p}{f}\right)^4\right] \gamma^{\exp\left[-(f-f_p)^2/\left(2\sigma_J^2 f_p^2\right)\right]}, \tag{2.1}$$

where g denotes the acceleration of gravity, α controls the significant wave height and σ_J is the asymmetry parameter: $\sigma_J = 0.07$ for $f < f_p$ and $\sigma_J = 0.09$ for $f > f_p$. The peak enhancement factor $\gamma = 3.3$ is fixed during the campaign. In total, 11 incident wave conditions were chosen according to preliminary numerical investigations of the UWO set-up (results not shown here). These wave conditions are tested in the experimental wave flume for the UWO set-up. The key parameters of the measurements are listed in table 1, including the peak period T_p, the significant wave height $H_s = 4\sqrt{m_0}$ (m_0 denoting the zeroth moment of the wave spectrum), the wave steepness $\epsilon = k_p a$ ($a = \sqrt{2m_0}$ and k_p is the wavenumber corresponding to the peak period) and the relative water depth $\mu = k_p h$, averaged over the upstream flat area or the bar crest area. Note that values of the Ursell number $Ur = \epsilon/\mu^3$ are not included in table 1 to limit the table size, but they can be easily calculated with the given values of ϵ and μ.

In the UWO tests, k_p is obtained from the peak frequency $\omega_p = 2\pi f_p$ by solving the dispersion relationship of linear waves:

$$\omega = 2\pi/T = \sqrt{gk \tanh(kh)}. \tag{2.2}$$

For each condition, five wave sequences with 10 min duration each were generated using different sets of random phases. For particular cases, we have tested ten wave sequences with random phases. The evolution trends of the statistical parameters are quite similar to those obtained with five sequences; we therefore anticipate that the results of five sequences have reached or are close to statistical convergence. For all the cases considered in this work, the values of incident steepness are set as moderate, such that no breaking occurs over the bar, even when freak waves appear.

These cases are of relative water depth below or around the transition depth, which was estimated according to a preliminary numerical study, and the NED is expected to manifest in the UWO tests. It should be mentioned that, in the preliminary numerical investigation, the transition depth for the occurrence of NED in the UWO set-up is approximately 0.9, considerably smaller than the 1.3 value reported in Trulsen *et al.* (2020). It is conjectured that the difference in the transition depth is mainly related to the upslope gradient of 1/30 used in this study, which is significantly smaller than the 1/3.81 slope in Trulsen *et al.* (2020).

	Upstream flat area (UWO/UWC)				Bar crest area (UWO/UWC)			
No.	T_p (s)	H_s (cm)	μ	ϵ	T_p (s)	H_s (cm)	μ	ϵ
1	1.38/1.38	5.6/4.9	2.18/2.00	0.043/0.034	1.38/1.38	5.0/3.9	1.07/0.90	0.047/0.031
2	1.48/1.49	6.6/5.8	1.91/1.76	0.044/0.036	1.49/1.50	5.9/4.8	0.97/0.82	0.050/0.035
3	1.60/1.60	6.4/5.8	1.69/1.58	0.038/0.032	1.60/1.60	5.8/4.8	0.88/0.76	0.045/0.032
4	1.79/1.78	7.3/6.5	1.41/1.35	0.036/0.031	1.81/1.80	6.7/5.6	0.76/0.67	0.045/0.033
5	2.12/2.14	9.0/8.4	1.11/1.05	0.036/0.031	2.15/2.17	8.7/7.5	0.63/0.54	0.048/0.036
6	2.24/2.27	9.1/8.7	1.03/0.97	0.033/0.030	2.27/2.30	8.8/7.9	0.59/0.51	0.046/0.035
7	2.35/2.38	9.2/8.7	0.97/0.92	0.031/0.028	2.39/2.41	8.8/8.0	0.56/0.48	0.043/0.034
8	2.45/2.48	11.0/10.8	0.92/0.87	0.036/0.033	2.50/2.51	10.8/10.1	0.53/0.46	0.051/0.041
9	2.54/2.57	10.2/10.2	0.88/0.83	0.032/0.030	2.57/2.58	10.0/9.6	0.51/0.45	0.046/0.038
10	2.86/—	10.0/—	0.76/—	0.027/—	2.89/—	10.0/—	0.45/—	0.040/—
11	3.17/—	7.9/—	0.68/—	0.019/—	3.16/—	8.1/—	0.41/—	0.030/—

Table 1. Key parameters in the UWO/UWC tests over upstream flat area ($h_1 = 1$ m) and bar crest area ($h_2 = 0.4$ m). The peak period T_p and significant wave height H_s are averaged measurements in each corresponding area. The wavenumber k_p is computed with the proper dispersion relationship (i.e. considering the local horizontal current velocity, if present).

The same incident wave trains of cases 1–9 were then tested under the UWC condition. The target current is uniform in the vertical direction yet varying in the horizontal direction due to the presence of the bar. The flow velocity U is set to $0.1\,\mathrm{m\,s^{-1}}$ in the upstream flat area, and the corresponding volume flux is $Q = Ubh_1 = 0.15\,\mathrm{m^3\,s^{-1}}$. Considering the conservation of Q along the flume, the local target flow velocity can be determined as $U(x) = Q/(bh(x))$. For validation, the UCO tests were conducted before the UWC tests and the horizontal flow velocity was measured with a Vectrino acoustic Doppler velocimeter from Nortek with a sampling frequency of 20 Hz. These flow measurements lasted for 10 min after the current became steady. Figure 2(*a*) shows the spatial evolution of the mean horizontal flow velocity with the standard deviation represented by error bars. Figure 2(*b*,*c*) presents the vertical profiles of horizontal flow velocity at two locations (before the bar and over the bar crest). The profiles of the target flow velocity are superimposed for comparison. These results indicate that the current was generated as desired.

Then, the UWC tests were performed. The key parameters of the UWC tests are also given in table 1, with k_p determined now via the Doppler-shifted dispersion relationship (Peregrine 1976):

$$\omega = \sigma + kU = \sqrt{gk\tanh(kh)} + kU, \tag{2.3}$$

where σ denotes the intrinsic wave frequency, and taking the lowest of the two positive roots for k.

Finally, the wave trains of cases 1–9 were tested under the FWO condition (with uniform depth h_1). The key parameters of the FWO tests are approximately equal to those in the upstream flat area of the UWO tests shown in table 1, thus not duplicated.

3. Results and analysis

3.1. *Effects of accelerating following current on wave statistics*

We focus on the effects induced by the current field in addition to effects of the variable seabed. The results shown are the mean of five samples in each case. The spatial evolutions

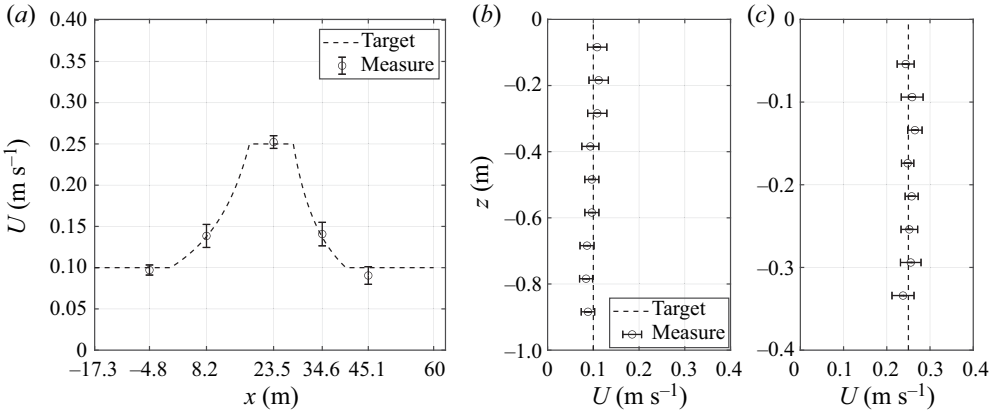

Figure 2. Mean horizontal flow velocity U measured in the UCO set-up. (*a*) Longitudinal evolution along the flume and vertical profiles measured at two abscissas: (*b*) $x = -4.8$ m (before the bar) and (*c*) $x = 23.5$ m (on the bar crest).

of three statistical parameters are shown: the significant wave height H_s, normalized by $H_{s,0}$, the significant wave height measured at the first probe of the corresponding FWO case; skewness $\lambda_3(\eta) = \langle(\eta - \langle\eta\rangle)^3\rangle/m_0^{3/2}$; and kurtosis $\lambda_4(\eta) = \langle(\eta - \langle\eta\rangle)^4\rangle/m_0^2$, with $\langle\cdot\rangle$ being the averaging operator. Skewness is a measure of wave profile asymmetry in the vertical direction and kurtosis is positively correlated with the freak wave occurrence probability. The local enhancements of these two parameters are seen as a sign of the non-equilibrium phenomenon (NEP) as waves propagate in non-homogeneous media.

Cases 1–9 are tested in the FWO, UWO and UWC scenarios. In figure 3, it is shown that the evolution of $H_s/H_{s,0}$ modulates within a limited range around the mean level, with no obvious decay in the FWO cases (black asterisks), indicating that the dissipation is negligible in such circumstances. However, the dissipation is non-trivial in the uneven bottom set-up: H_s is decreased by roughly 20 % after the bar in both UWO and UWC tests. The presence of a following current reduces H_s in comparison to the tests without current, and the reduction of H_s becomes less evident for longer waves, but more evident for shallower water depth where the current velocity is increased up to $0.25\,\mathrm{m\,s^{-1}}$. This can be explained by the principle of wave action conservation (Bretherton & Garrett 1969).

Figure 4 shows the evolution of λ_3. We see that in all the FWO tests, λ_3 remains approximately zero throughout the flume, as expected in a Gaussian sea state. In both UWO and UWC tests, cases 4–9 show evident local increase of λ_3, indicating the manifestation of NED over the bar crest. We notice that the following current further enhances the maximum value of λ_3 (see the red curves), and extends the region where λ_3 is enhanced. Besides, the spatial extent of the non-equilibrium area in the UWC tests increases for longer waves. In other words, a following current increases both the magnitude and the range of NED.

The evolution of λ_4 is shown in figure 5. The same trends as for λ_3 apply for λ_4. It is observed that in cases 3 and 4, the values of λ_4 get locally enhanced over the bar with the following current, whereas no such increase is noticeable in the corresponding UWO tests. For cases 5–9, the NEP is stronger in magnitude and lasts longer in space in the UWC scenario, in comparison with the UWO tests. Taking case 8 as an example, the maximum value of λ_4 is increased from 4.3 in the UWO set-up up to 5.0 in the UWC set-up.

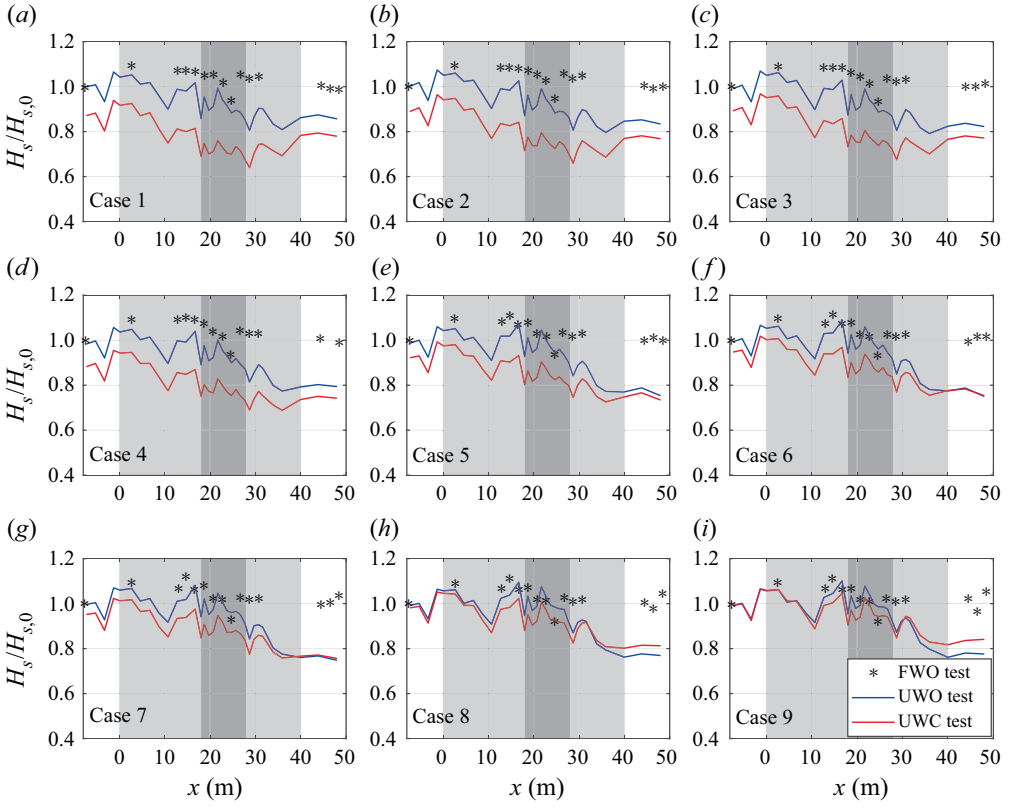

Figure 3. Evolution of normalized significant wave height $H_s/H_{s,0}$ in (*a–i*) cases 1–9 for FWO, UWO and UWC set-ups, with the bar profile indicated by grey areas.

This would imply a heavier tail in the wave height distribution, and therefore a higher freak wave probability.

It should be noticed that the MI is not responsible for the local increase of λ_3 and λ_4 in this study. For the UWC tests, in the upstream flat area with $h_1 = 1\,\mathrm{m}$ and $U_1 = 0.1\,\mathrm{m\,s^{-1}}$, the MI is expected to manifest for $k_p h_1 > 1.39$; over the bar crest with $h_2 = 0.4\,\mathrm{m}$ and $U_2 = 0.25\,\mathrm{m\,s^{-1}}$, the threshold for MI increases to $k_p h_2 > 1.48$ (see equation (41) in Liao *et al.* (2017)). For the UWO tests, the $k_p h$ threshold for MI is always 1.36. Therefore, waves in all cases are modulationally stable over the bar crest.

Undoubtedly, the UWC set-up considered in this study is complicated, involving wave–wave, wave–bottom, wave–current and current–bottom interactions. Based on the analysis of the threshold water depth with current effect taken into account, the MI is considered to be insignificant for the local increase of skewness and kurtosis over the bar crest. The uneven bottom could increase the vorticity of the fluid, but this could be omitted considering the gentleness of the slope.

The uneven bottom might also give rise to free-surface deformation when a pure (steady) current passes over, as a result of significant current–bottom interaction (e.g. Buttle *et al.* 2018; Akselsen & Ellingsen 2019). It should be pointed out that such current-induced free-surface deformation (CIFSD) is a steady solution, i.e. the CIFSD is time-independent when the steady state is achieved. The CIFSD can therefore be considered as a change of the local mean water level, resulting in a change of the local water depth. The wave

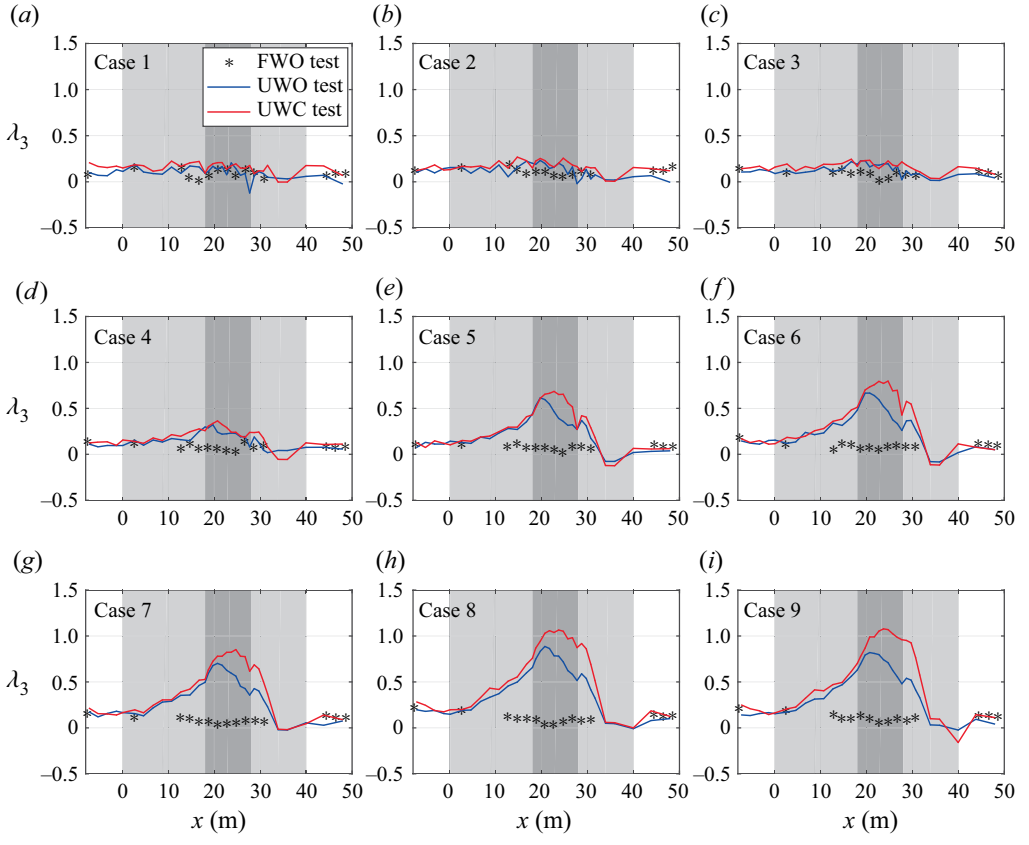

Figure 4. Evolution of skewness λ_3 in (*a–i*) cases 1–9 for FWO, UWO and UWC set-ups, with the bar profile indicated by grey areas.

evolution may therefore be influenced by the CIFSD. In the present study, the current was generated 10 min before the wave-paddle started to move, so the steady state of the flow field was achieved, and the steady profile of the CIFSD over the bar crest was well established. Following equation (2.4) in Buttle *et al.* (2018), the maximum magnitude of CIFSD is approximately 0.003 m for our experimental tests. As it represents a very small variation of the water depth over the bar crest ($0.003/h_2 < 1\,\%$), we consider that the contribution of CIFSD to the evolution of central moments like skewness and kurtosis is minor and can be safely neglected in our study. In all, it is considered that the presence of the uneven bottom gradually changes the mean horizontal flow velocity without changing the (near) uniformity of the horizontal flow velocity along the z axis, and that the occurrence of CIFSD does not contribute to the local changes of λ_3 and λ_4 over the bar.

We understand that the accelerating following current enhances and extends the local increase of λ_3 and λ_4 as follows. A following current affects the surface waves in two aspects: on the one hand, it decreases the significant wave height (conservation of wave action); on the other hand, it decreases the wavenumber (Doppler effect). Both the steepness ϵ and the relative water depth μ are therefore decreased. The relative water depth over the shallower region $k_p h_2$ plays a dominant role in the manifestation of NED, smaller $k_p h_2$ resulting in stronger NEP. Thus, it is understandable to observe higher levels of λ_3

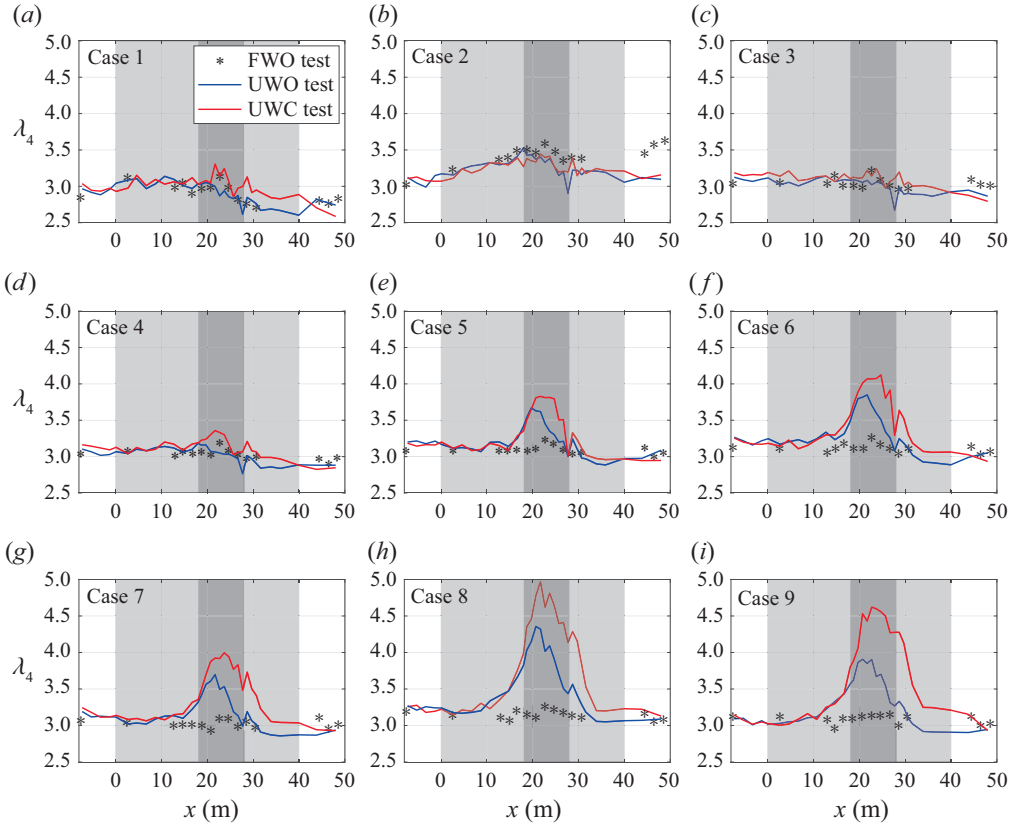

Figure 5. Evolution of kurtosis λ_4 in (a–i) cases 1–9 for FWO, UWO and UWC set-ups, with the bar profile indicated by grey areas.

and λ_4. Compared with the UWO tests, the following current in the UWC tests increases the level of medium inhomogeneity and a longer spatial distance is needed for the sea state to adapt to the new equilibrium state.

3.2. *Saturation depth for the maximum values of skewness and kurtosis*

Figure 6 further illustrates the relationship between the maximum values of λ_3, λ_4 (representing the magnitude of the NED) and the relative water depth $k_p h_2$ over the bar crest. The blue curve represents all 11 cases under the UWO condition and the red curve cases 1–9 under the UWC condition. Values of k_p are computed with the current velocity taken into account (using (2.3)). It is shown that the evolution trends of maximum values of λ_3 and λ_4 as functions of $k_p h_2$ are very similar in UWO and UWC scenarios (given k_p computed with proper dispersion relation). In our experiments, the NEP starts to appear for $k_p h_2 \approx 0.8$ (the above-mentioned 'transition' depth).

Furthermore, figure 6 shows that the increase of λ_3 and λ_4 with the decrease of $k_p h_2$ seems to stop for $k_p h_2 \approx 0.45$. This is not surprising since the increasing trend of λ_3 and λ_4 cannot be sustained unlimitedly. We refer to this particular relative water depth $k_p h_2 \approx 0.45$ as the 'saturation depth' of the NED. Below that saturation depth, λ_3 and λ_4 will no longer increase with a decrease of $k_p h_2$. As the peak period T_p increases, the relative water depth decreases throughout the flume. The difference between the shallower and the

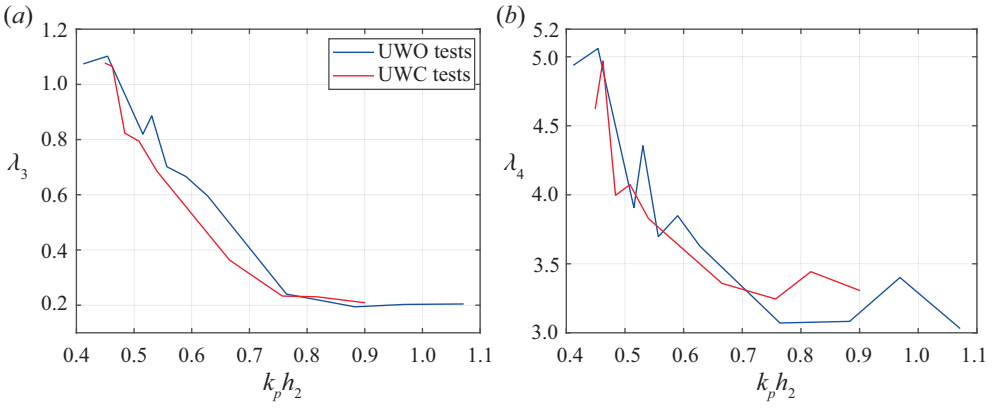

Figure 6. Maximum values of skewness (*a*) and kurtosis (*b*) over the shallower region as a function of the relative water depth over the bar crest.

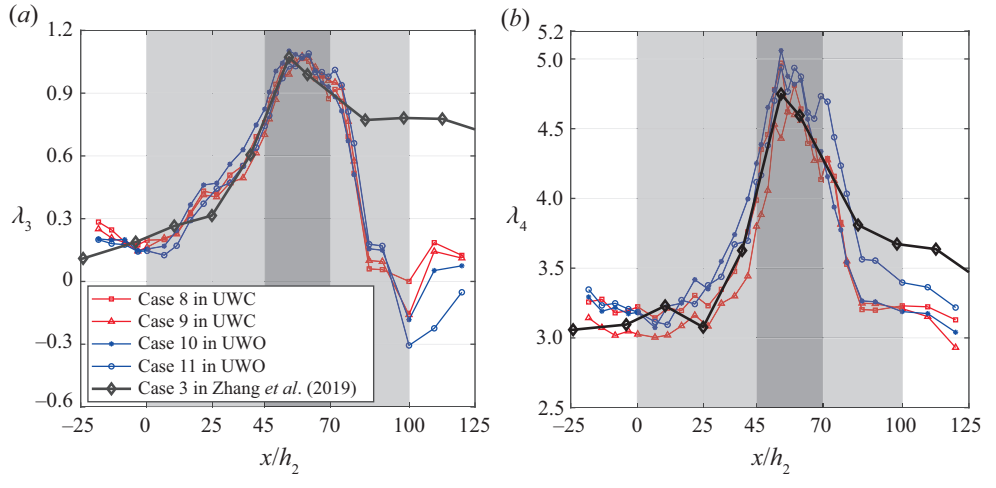

Figure 7. Evolution of skewness (*a*) and kurtosis (*b*) in cases 8–11, and in case 3 reported in Zhang *et al.* (2019). In all cases, $k_p h_2$ is below the saturation depth.

deeper depth (i.e. the change of condition) also reduces; therefore, the non-equilibrium responses are weakened and the increasing trends of λ_3 and λ_4 slow down as well.

The saturation depth has been indicated (without defining a terminology) in the theoretical work of Mendes *et al.* (2022), where those authors consider the enhancement of λ_3 and λ_4 takes place for $k_p h_2 \in [0.5, 1.5]$. Yet, such a saturation depth has never been reported in experimental works. It is anticipated that as the water depth decreases further, the wave evolution would be dominated by other effects, such as shallow-water effect and depth-induced breaking effect. Investigating these effects is certainly of academic and practical significance, yet it is beyond the present discussion of NED.

To further illustrate the 'saturation' effects, figure 7 superimposes the evolution of λ_3 and λ_4 in four cases: cases 8 and 9 in the UWC scenario and cases 10 and 11 in the UWO scenario. In all these cases, $k_p h_2$ is considered saturated. It can be observed that the spatial

profiles of λ_3 and λ_4 are very similar in these cases. Especially, the evolution of λ_3 is almost identical. When $k_p h_2$ saturates, in addition to similar maximum values of λ_3 and λ_4, we also notice that the following current does not result in a longer spatial range of NED. As a cross-validation for the saturation depth, we add in figure 7 one of the experimental results of Zhang *et al.* (2019), obtained in a wave flume of Tainan Hydraulics Laboratory (THL). In the THL experiments, the bathymetry is composed of two flat regions connected by a constant upslope (1/20). Here, we only take case 3 reported in Zhang *et al.* (2019), in which $k_p h_2$ happens to be 0.45 ($T_p = 2.5$ s, $h_2 = 0.3$ m, no current). In figure 7, the evolution of λ_3 and λ_4 of THL case 3 of Zhang *et al.* (2019) (black curves) is shifted in space, so that the positions of maximum λ_3 and λ_4 align with the present results. Despite considerably different configurations, the spatial profiles of λ_3 and λ_4 of THL case 3 are in good agreement with the present results. It should be understood that λ_3 keeps a high level after 30 m in THL case 3 because there is no de-shoaling process. Therefore, we speculate that the saturation depth $k_p h_2 \approx 0.5$ has some universal relevance, though this needs to be confirmed by additional investigations.

4. Conclusion

We experimentally investigated the NED of surface waves induced by medium inhomogeneity, here provoked by spatially varying water depth and current velocity. In this experimental campaign, 11 irregular wave conditions have been tested under FWO, UWO and UWC scenarios. The results show that a following current could amplify the medium inhomogeneity as waves propagate over a shoal, such that higher peaks and wider spatial extents of the local enhancement of skewness λ_3 and kurtosis λ_4 are achieved. The probability of freak waves is therefore enhanced due to an accelerating following current. This is because the decrease of the relative water depth can overwhelm the decrease of wave steepness, resulting in stronger sea-state NED response over a larger spatial extent. The maximum values of λ_3 and λ_4 achieved over the bar crest increase with the decrease of $k_p h_2$ in the UWO tests, and the relationships hold for the UWC tests with k_p evaluated with the current velocity taken into account.

The evolution of maximum λ_3 and λ_4 as functions of $k_p h_2$ shows two particular thresholds of relative depth: one is the so-called 'transition depth' (Trulsen *et al.* 2020), below which the NED starts to manifest (approximately 0.8 in our experimental set-up); the other one is approximately 0.45–0.5, below which the maximum λ_3 and λ_4 no longer increase with a further decrease of $k_p h_2$, the latter being named 'saturation depth'. To the best of our knowledge, this saturation depth has never been reported in previous experimental works.

The present results are of high practical importance, especially for the assessment of freak wave risks in coastal areas with ambient currents. We have demonstrated that, somewhat counter-intuitively, a following current entering a shallow-water area increases the risk of extreme waves in that area.

Acknowledgements. The authors are grateful to the three anonymous reviewers for their valuable suggestions on various aspects that have considerably improved the paper, in particular on the discussion of CIFSD.

Funding. This work was supported by the National Natural Science Foundation of China (grant nos. 52101301; 51720105010), the China Postdoctoral Science Foundation (grant no. 2021M690523) and the Innovative Research Foundation of Ship General Performance (grant no. 31422119).

Declaration of interests. The authors report no conflict of interest.

Author ORCIDs.
Jie Zhang https://orcid.org/0000-0003-0794-2335;
Yuxiang Ma https://orcid.org/0000-0003-4314-0428;
Michel Benoit https://orcid.org/0000-0003-4195-2983.

References

Adcock, T.A.A. & Taylor, P.H. 2014 The physics of anomalous ('rogue') ocean waves. *Rep. Prog. Phys.* **77**, 105901.

Akhmediev, N. & Pelinovsky, E. 2010 Editorial – introductory remarks on 'Discussion & debate: rogue waves – towards a unifying concept?' *Eur. Phys. J.* **185**, 1–4.

Akselsen, A.H. & Ellingsen, S.Å. 2019 Sheared free-surface flow over three-dimensional obstructions of finite amplitude. *J. Fluid Mech.* **878**, 740–767.

Benjamin, T.B. 1967 Instability of periodic wavetrains in nonlinear dispersive systems. *Proc. R. Soc.* A **299**, 59–76.

Bretherton, F.P. & Garrett, C.J.R. 1969 Wavetrains in inhomogeneous moving media. *Proc. Math. Phys. Engng Sci.* **302**, 529–554.

Buttle, N.R., Pethiyagoda, R., Moroney, T.J. & McCue, S.W. 2018 Three-dimensional free-surface flow over arbitrary bottom topography. *J. Fluid Mech.* **846**, 166–189.

Chawla, A. & Kirby, J.T. 2002 Monochromatic and random wave breaking at blocking points. *J. Geophys. Res.* **107**, 3067.

Curtis, C.W. & Murphy, M. 2020 Evolution of spectral distributions in deep-water constant vorticity flows. *Water Waves* **2**, 361–380.

Dematteis, G., Grafke, T., Onorato, M. & Vanden-Eijnden, E. 2019 Experimental evidence of hydrodynamic instantons: the universal route to rogue waves. *Phys. Rev.* X **9**, 041057.

Ducrozet, G., Abdolahpour, M., Nelli, F. & Toffoli, A. 2021 Predicting the occurrence of rogue waves in the presence of opposing currents with a high-order spectral method. *Phys. Rev. Fluids* **6**, 064803.

Ducrozet, G. & Gouin, M. 2017 Influence of varying bathymetry in rogue wave occurrence within unidirectional and directional sea-states. *J. Ocean Engng Mar. Energy* **3**, 309–324.

Dysthe, K., Krogstad, H.E. & Müller, P. 2008 Oceanic rogue waves. *Annu. Rev. Fluid Mech.* **40**, 287–310.

Fedele, F., Brennan, J., Ponce de León, S., Dudley, J. & Dias, F. 2016 Real world ocean rogue waves explained without the modulational instability. *Sci. Rep.* **6**, 27715.

Gerber, M. 1987 The Benjamin–Feir instability of a deep-water Stokes wavepacket in the presence of a non-uniform medium. *J. Fluid Mech.* **176**, 311–332.

Gramstad, O., Zeng, H., Trulsen, K. & Pedersen, G.K. 2013 Freak waves in weakly nonlinear unidirectional wave trains over a sloping bottom in shallow water. *Phys. Fluids* **25**, 122103.

Hjelmervik, K.B. & Trulsen, K. 2009 Freak wave statistics on collinear currents. *J. Fluid Mech.* **637**, 267–284.

Kashima, H. & Mori, N. 2019 Aftereffect of high-order nonlinearity on extreme wave occurrence from deep to intermediate water. *Coast. Engng* **153**, 103559.

Kharif, C., Kraenkel, R.A., Manna, M.A. & Thomas, R. 2010 The modulational instability in deep water under the action of wind and dissipation. *J. Fluid Mech.* **664**, 138–149.

Kharif, C. & Pelinovsky, E. 2003 Physical mechanisms of the rogue wave phenomenon. *Eur. J. Mech. (B/Fluids)* **22**, 603–634.

Lavrenov, I.V. & Porubov, A.V. 2006 Three reasons for freak wave generation in the non-uniform current. *Eur. J. Mech. (B/Fluids)* **25**, 574–585.

Lawrence, C., Trulsen, K. & Gramstad, O. 2021 Statistical properties of wave kinematics in long-crested irregular waves propagating over non-uniform bathymetry. *Phys. Fluids* **33**, 046601.

Lawrence, C., Trulsen, K. & Gramstad, O. 2022 Extreme wave statistics of surface elevation and velocity field of gravity waves over a two-dimensional bathymetry. *J. Fluid Mech.* **939**, A41.

Li, Y., Draycott, S., Adcock, T.A.A. & van den Bremer, T.S. 2021*a* Surface wavepackets subject to an abrupt depth change. Part 2. experimental analysis. *J. Fluid Mech.* **915**, A72.

Li, Y., Draycott, S., Zheng, Y., Lin, Z., Adcock, T.A.A. & van den Bremer, T.S. 2021*b* Why rogue waves occur atop abrupt depth transitions. *J. Fluid Mech.* **919**, R5.

Li, Y., Zheng, Y., Lin, Z., Adcock, T.A.A. & van den Bremer, T.S. 2021*c* Surface wavepackets subject to an abrupt depth change. Part 1. second-order theory. *J. Fluid Mech.* **915**, A71.

LIAO, B., DONG, G., MA, Y. & GAO, J.L. 2017 Linear-shear-current modified Schrödinger equation for gravity waves in finite water depth. *Phys. Rev.* E **96**, 043111.

LONGUET-HIGGINS, M.S. & STEWART, R.W. 1961 The changes in amplitude of short gravity waves on steady non-uniform currents. *J. Fluid Mech.* **10**, 529–549.

MA, Y., CHEN, H., MA, X. & DONG, G. 2017 A numerical investigation on nonlinear transformation of obliquely incident random waves on plane sloping bottoms. *Coast. Engng* **130**, 65–84.

MA, Y., DONG, G., PERLIN, M., MA, X., WANG, G. & XU, J. 2010 Laboratory observations of wave evolution, modulation and blocking due to spatially varying opposing currents. *J. Fluid Mech.* **661**, 108–129.

MA, Y., MA, X. & DONG, G. 2015 Variations of statistics for random waves propagating over a bar. *J. Mar. Sci. Technol.* **23**, 864–869.

MENDES, S., SCOTTI, A., BRUNETTI, M. & KASPARIAN, J. 2022 Non-homogeneous analysis of rogue wave probability evolution over a shoal. *J. Fluid Mech.* **939**, A25.

ONORATO, M., PROMENT, D. & TOFFOLI, A. 2011 Triggering rogue waves in opposing currents. *Phys. Rev. Lett.* **107**, 184502.

ONORATO, M., RESIDORI, S., BORTOLOZZO, U., MONTINA, A. & ARECCHI, F.T. 2013 Rogue waves and their generating mechanisms in different physical contexts. *Phys. Rep.* **528**, 47–89.

ONORATO, M. & SURET, P. 2016 Twenty years of progresses in oceanic rogue waves: the role played by weakly nonlinear models. *Nat. Hazards* **84**, 541–548.

PEREGRINE, D.H. 1976 Interaction of water waves and currents. In *Advances in Applied Mechanics* (ed. C.-S. Yih), pp. 9–117. Elsevier.

STOCKER, J.R. & PEREGRINE, D.H. 1999 The current-modified nonlinear Schrödinger equation. *J. Fluid Mech.* **399**, 335–353.

TOFFOLI, A., *et al.* 2013 Experimental evidence of the modulation of a plane wave to oblique perturbations and generation of rogue waves in finite water depth. *Phys. Fluids* **25**, 091701.

TOFFOLI, A., CAVALERI, L., BABANIN, A.V., BENOIT, M., BITNER-GREGERSEN, E.M., MONBALIU, J., ONORATO, M., OSBORNE, A.R. & STANSBERG, C.T. 2011 Occurrence of extreme waves in three-dimensional mechanically generated wave fields propagating over an oblique current. *Nat. Hazards Earth Syst. Sci.* **11**, 895–903.

TOFFOLI, A., WASEDA, T., HOUTANI, H., CAVALERI, L., GREAVES, D. & ONORATO, M. 2015 Rogue waves in opposing currents: an experimental study on deterministic and stochastic wave trains. *J. Fluid Mech.* **769**, 277–297.

TRULSEN, K. 2018 Rogue waves in the ocean, the role of modulational instability, and abrupt changes of environmental conditions that can provoke non equilibrium wave dynamics. In *The Ocean in Motion* (ed. M.G. Velarde, R.Y. Tarakanov & A.V. Marchenko), pp. 239–247. Springer International Publishing.

TRULSEN, K., RAUSTØL, A., JORDE, S. & RYE, L.B. 2020 Extreme wave statistics of long-crested irregular waves over a shoal. *J. Fluid Mech.* **882**, R2.

TRULSEN, K., ZENG, H. & GRAMSTAD, O. 2012 Laboratory evidence of freak waves provoked by non-uniform bathymetry. *Phys. Fluids* **24**, 097101.

VORONOVICH, V.V., SHRIRA, V.I. & THOMAS, G. 2008 Can bottom friction suppress 'freak wave' formation? *J. Fluid Mech.* **604**, 263–296.

WHITE, B.S. & FORNBERG, B. 1998 On the chance of freak waves at sea. *J. Fluid Mech.* **355**, 113–138.

ZENG, H. & TRULSEN, K. 2012 Evolution of skewness and kurtosis of weakly nonlinear unidirectional waves over a sloping bottom. *Nat. Hazards Earth Syst. Sci.* **12**, 631–638.

ZHANG, J. & BENOIT, M. 2021 Wave–bottom interaction and extreme wave statistics due to shoaling and de-shoaling of irregular long-crested wave trains over steep seabed changes. *J. Fluid Mech.* **912**, A28.

ZHANG, J., BENOIT, M., KIMMOUN, O., CHABCHOUB, A. & HSU, H.-C. 2019 Statistics of extreme waves in coastal waters: large scale experiments and advanced numerical simulations. *Fluids* **4**, 99.

ZHANG, J., BENOIT, M. & MA, Y. 2022 Equilibration process of out-of-equilibrium sea-states induced by strong depth variation: evolution of coastal wave spectrum and representative parameters. *Coast. Engng* **174**, 104099.

ZHENG, Y., LIN, Z., LI, Y., ADCOCK, T.A.A., LI, Y. & VAN DEN BREMER, T.S. 2020 Fully nonlinear simulations of unidirectional extreme waves provoked by strong depth transitions: the effect of slope. *Phys. Rev. Fluids* **5**, 064804.